Rabphilin-3A negatively regulates neuropeptide release, through its SNAP25 interaction

Rein I. Hoogstraaten[1*], Adlin Abramian[1*], Fiona H. Murphy[1], Kathryn F. mcDaniel[1], Ruud F. Toonen[1], Matthijs Verhage[1,2]

These authors contributed equally to this work.

[1]*Department of Functional Genomics, Faculty of Exact Science, Center for Neurogenomics and Cognitive Research, Vrije Universiteit Amsterdam and Vrije Universiteit Medical Center, Amsterdam 1081 HV, The Netherlands.*

[2]*Department of Clinical Genetics, Center for Neurogenomics and Cognitive Research, Amsterdam Neuroscience, Vrije Universiteit Medical Center, Amsterdam 1105 AZ, The Netherlands.*

To whom correspondence should be addressed: Matthijs Verhage, PhD (matthijs@cncr.vu.nl) or Ruud Toonen, PhD (ruud.toonen@cncr.vu.nl)

Abstract

Neuropeptides and neurotrophins are stored in and released from dense-core vesicles (DCVs). While DCVs and synaptic vesicles (SVs) share fundamental SNARE/SM proteins for exocytosis, a detailed understanding of DCV exocytosis remains elusive. We recently identified the RAB3-RIM1 pathway to be essential for DCV-, but not SV exocytosis, highlighting a significant distinction between the SV- and DCV secretory pathways. Whether RIM1 is the only RAB3 effector that is essential for DCV release is currently unknown. In this study, we characterized the role of rabphilin-3A (RPH3A), a known downstream effector of RAB3A, in the DCV secretory pathway using RPH3A-deficient hippocampal mouse neurons. RPH3A did not travel with DCVs, but remained stationary at synapses. In the absence of RPH3A, the number of DCV exocytosis events was 3-fold higher than in wildtype (WT) neurons. RPH3A lost its punctate distribution when it was unable to bind RAB3A. However, this was not rate limiting, as expressing a mutant RPH3A that was unable to bind RAB3A restored exocytosis to WT levels, but not when RPH3A was unable to bind SNAP25. In addition, RPH3A null neurons had longer neurites, which was partly restored when ablating all regulated secretion with tetanus neurotoxin. Taken together, we conclude that RPH3A negatively regulates DCV exocytosis, potentially also affecting neuron size. Furthermore, RAB3A interaction is required for the synaptic enrichment of RPH3A, but not for limiting DCV exocytosis. Instead the interaction of RPH3A with SNAP25 is relevant for inhibiting DCV exocytosis.

Introduction

Neuropeptides and neurotrophins are crucial neuronal signaling molecules that play diverse roles in brain development, neurogenesis and synaptic plasticity (Malva et al., 2012; Pang et al., 2004; Park & Poo, 2013; van den Pol, 2012; Zaben & Gray, 2013). These neuromodulators are sorted at the trans-Golgi network (TGN) and packaged into dense core vesicles (DCVs). Similar to neurotransmitter release from synaptic vesicles (SVs), neuropeptide release is calcium and activity-dependent. However, unlike SVs, DCVs can fuse at various locations in the neuron, requiring higher and more sustained stimulation frequencies (Balkowiec & Katz, 2002; Hartmann et al., 2001; Persoon et al., 2018). Interestingly, all SNARE/SM proteins essential for exocytosis are shared between these two secretory pathways (Arora

et al., 2017; Farina et al., 2015; Hoogstraaten et al., 2020; Puntman et al., 2021; Südhof, 2013; van de Bospoort et al., 2012). However, while SV secretory pathways are well characterized, a detailed understanding of DCV exocytosis is still emerging. We recently discovered that RAB3, a protein largely dispensable for SV exocytosis (Schlüter et al., 2004, 2006), and its effector RIM1 to be essential for DCV exocytosis (Persoon et al., 2019). This indispensable role of the RAB3-RIM pathway signifies a main difference between SV and DCV exocytosis. Whether RIM is the only RAB3 effector that is essential for DCV exocytosis is currently unknown.

Rabphilin-3A (RPH3A) is a downstream effector of RAB3A and highly expressed in the brain (Schlüter et al., 1999). RPH3A binds RAB3A and RAB27 and contains two lipid- and calcium-binding C2 domains (Guillén et al., 2013; Tsuboi & Fukuda, 2005). The second C2 domain (C2B) binds SNAP25 in a calcium independent manner (Deák et al., 2006). Similar to RAB3 null mutants, depletion of RPH3A shows no detectable synaptic phenotype in mice under normal physiological conditions (Schlüter et al., 1999), and only a mild phenotype in *C. elegans* (Staunton et al., 2001). However, mutant mice do show increased synaptic recovery after intense stimulation, which is rescued by reintroducing full length (FL) RPH3A but not a mutant that lacks the C2B domain. This suggests that RPH3A negatively regulates SV recycling after depletion of the releasable vesicle pool, and that this function depends on its SNAP25 interaction (Deák et al., 2006). In C. *elegans*, the absence of RBF-1, the homolog of RPH3A, exacerbates the phenotypes of other SNARE mutants, as observed in the *rbf-1/ric-4* (RPH3A/SNAP25) double mutant, suggesting that RPH3A contributes to SNARE protein function (Staunton et al., 2001).

The role of RPH3A in the context of DCV exocytosis within mammalian neurons remains unclear. Notably, a recent genetic screen in C. *elegans* revealed that *rbf-1* depletion increases the release of fluorescently tagged neuropeptides without affecting the frequency of spontaneous mini-EPSCs. This suggest a potential negative regulatory role for RPH3A in neuropeptide release (Laurent et al., 2018), opposite to RIM1 (Persoon et al., 2019). However, it remains uncertain whether RPH3A functions as a negative regulator in mammalian neurons, and whether, similar as in synaptic transmission, the interaction with SNAP25 is important in this.

We set out to determine the role of RPH3A in DCV exocytosis in hippocampal mouse neurons, and to investigate the relevance of RAB3A and SNAP25 binding in this. We found that RPH3A did not travel with DCVs, but remained stationary at synapses. Using RPH3A null mutant mice (Schlüter et al., 1999) we show that the absence of RPH3A indeed increased DCV exocytosis. Furthermore, RPH3A null neurons exhibit longer neurites and increased number of DCVs. This effect was partly reduced when all regulated secretion was eliminated by tetanus neurotoxin (TeNT) (Hoogstraaten et al., 2020; Shimojo et al., 2015), indicating that the increased neurite length partially depends on regulated secretion. Finally, expressing a mutant RPH3A unable to bind RAB3A/RAB27A restored DCV exocytosis, but not when expressing a mutant RPH3A unable to bind SNAP25. This suggests that limiting DCV exocytosis does not depend on the interaction with RAB3A, but at least in part on the interaction with SNAP25.

Results

RPH3A localizes to synapses and does not travel with DCVs

RPH3A is reported to localize to both pre- and post-synaptic sites (Stanic et al., 2015), and on DCVs through its RAB-binding domain (RBD) in PC12 cells (Fukuda et al., 2004). To assess whether RPH3A

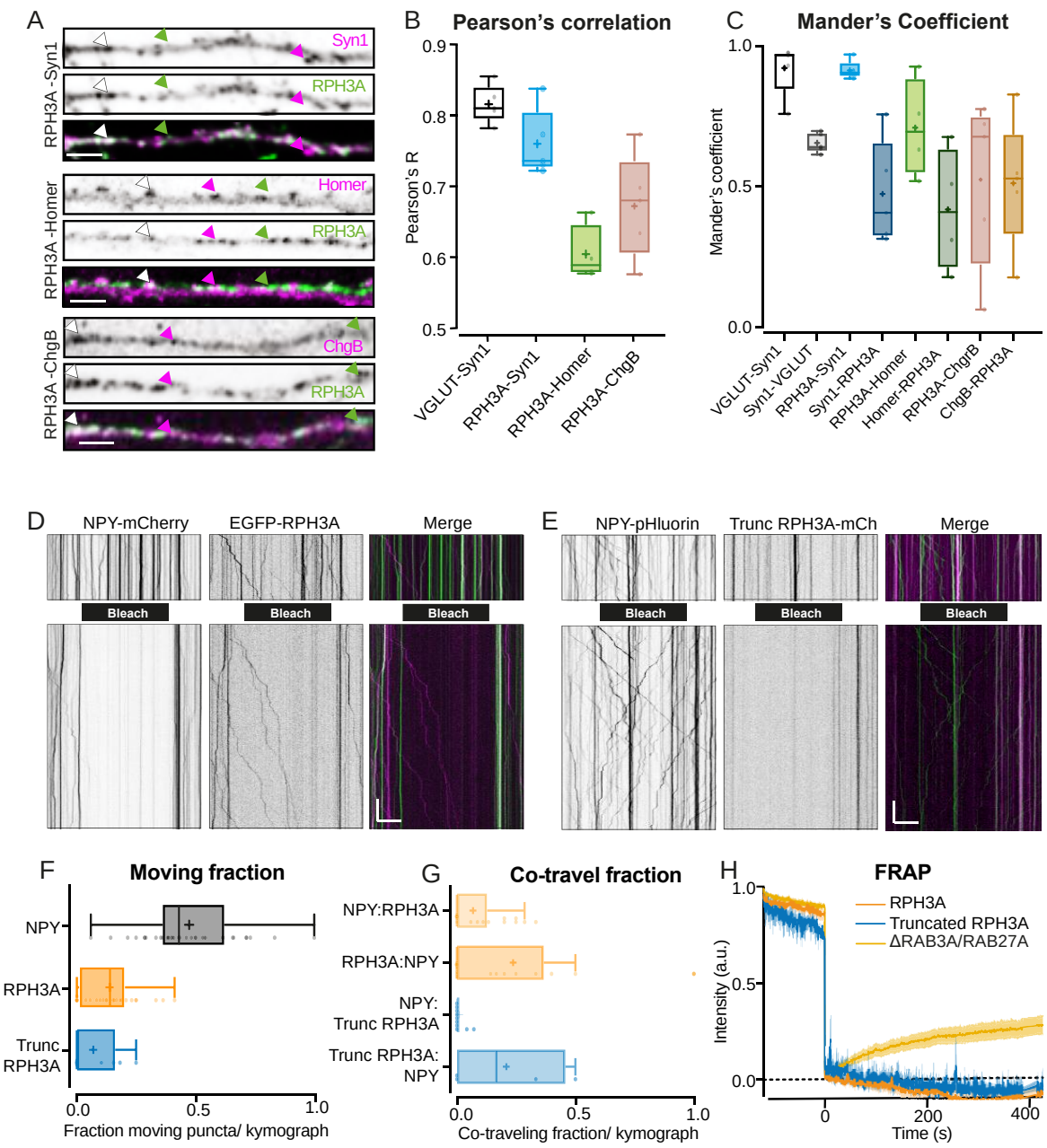

Figure 1. RPH3A localizes to synapses and does not travel on DCVs. (**A**) Neurites co-stained for RPH3A (green) and Synapsin-1, Homer, or ChgB (all magenta). White arrows indicate co-localizing puncta whereas green and magenta arrows indicate single RPH3A or Syn1/Homer/ChgB puncta, respectively. Scale bar, 5 µm. (**B**) Pearson's correlation coefficient and (**C**) Mander's overlap coefficient for each condition including VGLUT1 and syn1 as positive controls. Dots represent a field of view. (**D**) Kymographs of EGFP-RPH3A and NPY-mCherry, and (**E**) mCherry-truncated RPH3A and NPY-pHluorin before (upper) and after (lower) photobleaching (black bar). Merge images show mCherry (pseudo-colored magenta) and EGFP/pHluorin (green). Scale bar, 20 µm (x-axis) and 20 s (y-axis). (**F**) Moving fraction of NPY and FL or truncated RPH3A puncta per kymograph. (**G**) Fraction of moving NPY puncta with FL or truncated RPH3A puncta, and moving FL/truncated RPH3A with NPY puncta. Dots represent a kymograph. (**H**) Fluorescent recovery traces after photobleaching of RPH3A, truncated RPH3A and ΔRAB3A/RAB27A RPH3A. Lines ± shading represents mean ± SEM. Boxplots represent median (line), mean (+) and Tukey range (whiskers).

is present on DCVs in hippocampal mouse neurons, we immunostained for RPH3A and the DCV marker chromogranin B (ChgB) at 16 days *in vitro* (DIV16) (Figure 1A). To validate the cellular localization of RPH3A, neurons were immunostained for pre-synaptic marker Synapsin1 (Syn1), and postsynaptic marker Homer (Figure 1A). RPH3A immunostaining was mostly punctate and colocalized with Syn1 and, to a lesser extent, with Homer and ChgB (Figure 1B), but not all Syn1 puncta contained RPH3A (Figure

1C). Similarly, RPH3A immunostaining overlapped with a subset of postsynaptic puncta (Figure 1C). A mutant RPH3A that was unable to bind RAB3A/RAB27A (ΔRAB3A/RAB27A) (Fukuda et al., 2004), lost the punctate distribution (Figure S1A, B). However, this was not the case with a mutant RPH3A that cannot bind SNAP25 (ΔSNAP25) (Ferrer-Orta et al., 2017) or with other RPH3A mutants lacking specific interactions (Figure S1A-C). We confirmed that the neurite RPH3A expression was similar between the mutant RPH3A constructs and the FL RPH3A (Figure S1E, F). These data indicate that RPH3A is highly enriched at a subset of synapses, partly co-localizes with DCVs, and that the interaction with RAB3A, but not SNAP25, is required for its normal localization.

Recent evidence has demonstrated that RAB3A is transported along with DCVs (Persoon et al., 2019). To test if RPH3A travels together with DCVs, we co-expressed neuropeptide Y (NPY)-mCherry and EGFP-RPH3A (Tsuboi & Fukuda, 2005) in DIV14 RPH3A knockout (KO) neurons (Figure 1D). In addition, we tested co-transport of NPY-pHluorin with two RPH3A mutants, a truncated RPH3A lacking both C2 domains but retaining the RAB3A and RAB27A binding sites, and ΔRAB3A/RAB27A mutant (Fukuda et al., 2004) (Figure S1A). Live-cell imaging was performed before and after photobleaching a fixed-size area on a neurite to visualize vesicles entering the bleached area (Figure 1E). The number of moving versus immobile puncta was determined for each construct prior to photobleaching. Both FL- and truncated RPH3A exhibited high immobility (7-14% moving), although they occasionally showed small movements over short distances (less than 10 µm within 4 minutes). In contrast, 47% of NPY puncta were mobile (Figure 1F), as shown before (Hoogstraaten et al., 2020; Persoon et al., 2019). Only a small fraction of RPH3A (14%) and truncated RPH3A (7%) puncta travelled at velocities characteristic for DCV transport (Bittins et al., 2010; de Wit et al., 2006; Kwinter et al., 2009). These results indicate that the majority of RPH3A organizes in immobile puncta that colocalize with synaptic markers (see above), but do not travel through the neurites like DCVs do.

We next determined the fraction of RPH3A that traveled together with NPY-labelled vesicles by photobleaching stretches of neurites to enhance visualization of moving vesicles. Few moving NPY vesicles contained RPH3A or truncated RPH3A (NPY: RPH3A = 6%, NPY:Truncated RPH3A = 1%) and conversely, of the already small fraction of moving FL- and truncated RPH3A, only a few travelled together with NPY (RPH3A:NPY = 18%, truncated RPH3A:NPY = 8%; Figure 1G). ΔRAB3A/RAB27A RPH3A expression produced a more diffuse, gradual recovery after photobleaching (Figure 1H). Overall, these findings suggest that RPH3A predominantly localizes to a subset of synapses and does not travel with DCVs. In addition, the punctate organization of RPH3A relies on RAB3/RAB27 interactions.

RPH3A deficiency increases DCV exocytosis

Since RPH3A appeared to remain mostly stationary at the pre-synapse (Figure 1), we examined the role of RPH3A in neuropeptide release in hippocampal neurons. We recorded DCV fusion events in single hippocampal mouse neurons from RPH3A KO and wildtype (WT) littermates at DIV14-16. We confirmed the loss of RPH3A expression in RPH3A KO neurons (Figure 2A, B). NPY fused to pH-sensitive EGFP (NPY-pHluorin), a validated DCV fusion reporter (Arora et al., 2017; Farina et al., 2015; Persoon et al., 2018; van de Bospoort et al., 2012), was used to quantify single fusion events (Figure 2C). To elicit DCV fusion, neurons were stimulated twice with 8 X 50 action potential (AP) bursts at 50 Hz (interspaced by 0.5 s), separated by 30 s (Figure 2D) or once with 16 X 50 APs at 50Hz. To determine the total number

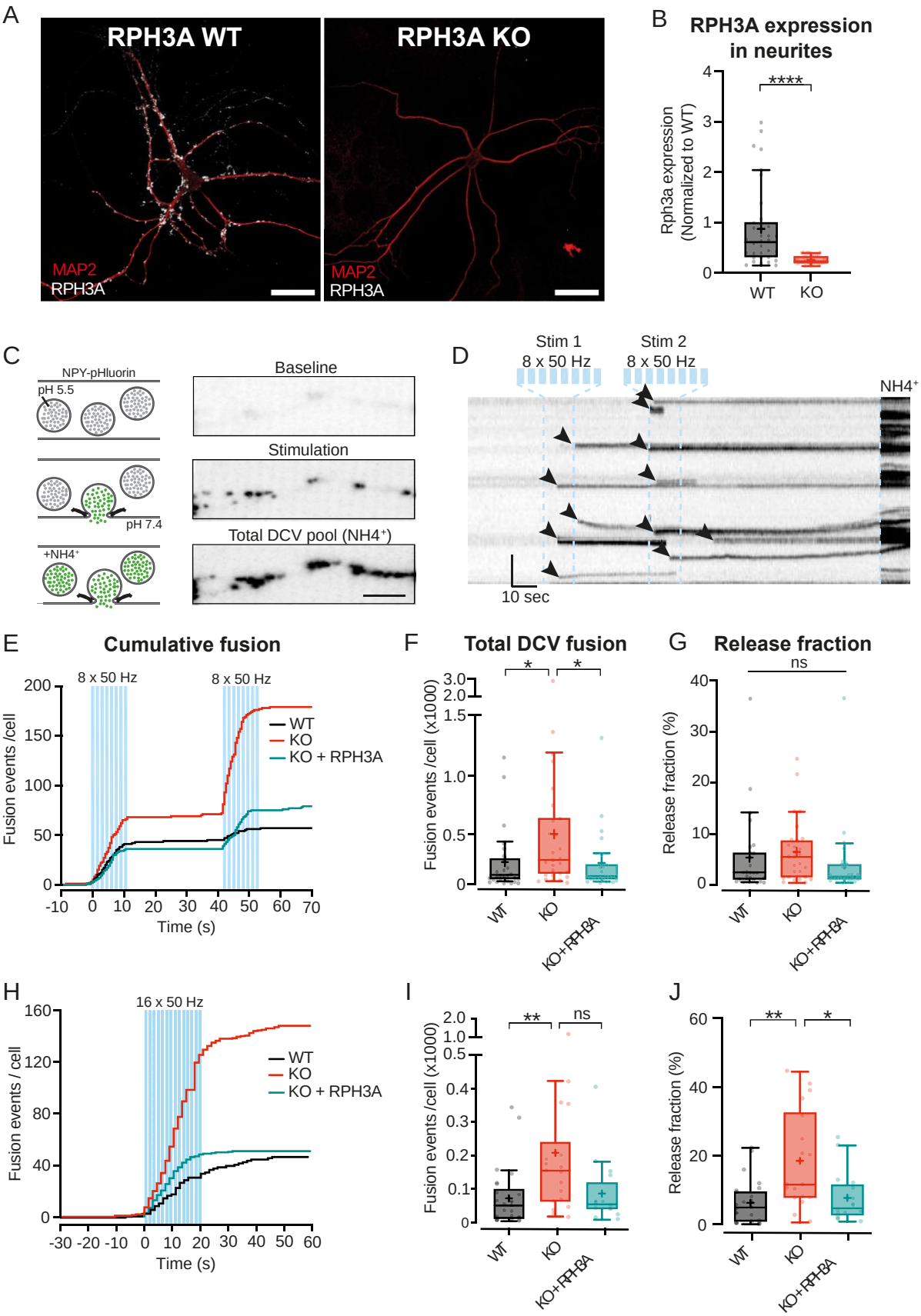

Figure 2. RPH3A deficiency increases DCV exocytosis. (**A**) Typical example of RPH3A WT and KO neurons stained for MAP2 (red) and RPH3A (white). Scale bar, 50 µm. (**B**) RPH3A expression in neurites of WT and KO neurons normalized to WT per independent experiment. N numbers of individual experiments and single neuron observations in brackets: WT: 4(34); KO: 4(33). (**C**) Schematic representation (left) and imaging example of a neurite stretch (right) infected with NPY-pHluorin as optical DCV fusion reporter. NPY-phluorin is quenched in the acidic DCV lumen before fusion (baseline) but dequenches upon fusion (stimulation). $NH4^+$ superfusion dequenches all NPY-pHluorin labeled DCVs (total DCV pool). Scale bar, 5 µm. (**D**) Kymograph of the neurite stretch with the stimulation

paradigm used to elicit DCV fusion (two bursts of 8 X 50 AP trains at 50 Hz interspaced by 0.5 second between each train and 30 seconds between each burst, blue bars) and NH4 superfusion ($NH4^+$) used to dequench all NPY-pHluorin labeled vesicles. Arrowheads indicate fusion events. (**E**) Cumulative median histogram of fusion events over time in WT (black), RPH3A KO (red) and KO neurons infected with FL RPH3A (cyan). Blue bars indicate the stimulation paradigm (8 x 50 AP bursts at 50 Hz). (**F**) Total DCV fusion events per condition (2x8 x 50 AP bursts at 50 Hz). N numbers of individual experiments and single neuron observations in brackets: WT: 5(51); KO: 5(43); KO + RPH3A: 5(39). (**G**) Released fraction defined as the number of fusion events normalized to the total pool of DCVs. (**H**) Cumulative median histogram of events over time in WT (black), RPH3A KO (red) and KO neurons infected with FL RPH3A (cyan). Blue bars indicate the stimulation paradigm (16 x 50 AP bursts at 50 Hz). (**I**) Number of DCV fusion events per condition (16 x 50 AP bursts at 50 Hz). N numbers of individual experiments and single neuron observations in brackets: WT: 4(25); KO: 4(18); KO + RPH3A: 4(16). (**J**) Release fraction per cell. Boxplots represent the median (line), mean (+) and Tukey range (whiskers). Each dot represents an individual neuron. Kruskal-Wallis H test with Dunn's correction: * $P < 0.05$, ** $P < 0.01$. ns = non-significant, $P > 0.05$.

of DCVs per cell, neurons were briefly superfused with NH_4^+ after stimulation to dequence all NPY-pHluorin labelled DCVs (Figure 2C, D).

RPH3A KO neurons showed a 3-fold increase in the total number of fusion events compared to WT (Figure 2E, F, S2A, B). To test if re-expressing RPH3A in KO neurons could restore DCV fusion to WT levels, we infected KO neurons with a FL RPH3A construct at DIV0 (Figure S1A). Similar to endogenous RPH3A expression (Figure 1A-C), this construct localized to synapses (Figure S1D). Overexpression of RPH3A in KO neurons restored the number of fusion events to WT levels (Figure 2E, F). A trend towards a larger intracellular DCV pool in KO compared to WT neurons was observed (Figure S2C). In line with this, the released fraction, i.e. the number of fusion events normalized to the total pool of DCVs, did not differ between WT and KO neurons (Figure 2G). During stronger stimulation (16 bursts of 50 APs at 50 Hz), the total fusion and released fraction of DCVs were increased in KO neurons compared to WT (Figure 2H, I). Overexpression of FL RPH3A in KO neurons again restored the number and released fraction of fusion events to WT levels (Figure 2H-J). No difference in DCV pool size was observed between WT and KO neurons (Figure S2D). Together, these findings indicate that RPH3A is an inhibitor of DCV exocytosis.

RPH3A deficiency leads to increased neurite length and DCV numbers

Since we observed a trend towards a bigger DCV pool in KO neurons (Figure S2C), and the total number of DCVs per neuron correlates with dendrite length (Persoon et al., 2018), we examined the neuronal morphology of RPH3A KO neurons. Single hippocampal neurons (DIV14) were immunostained for MAP2 to quantify the total dendrite length, and for DCV cargo ChgB to determine the number of DCVs (Figure 3A). Indeed, neurons lacking RPH3A had longer dendrites that harbored more DCVs than WT neurons (Figures 3B, C) and KO neurons contained more DCVs per µm (Figure 3D). The number of DCVs correlated with the total dendrite length in both genotypes (Figure 3F), as shown previously for WT neurons (Persoon et al., 2018). Moreover, the intensity of endogenous ChgB was decreased in RPH3A KO neurons, indicating affected vesicle loading or reduced clustering (Figure 3E), yet the peak intensity of fusion events during live recording was unchanged, suggesting that the decrease in DCV cargo intensity is more likely due to reduced clustering (Figure S2E). Taken together, these results suggest that lack of RPH3A leads to longer dendrites with a concomitant increase in the number of DCVs. However, RPH3A depletion does not seem to affect the neuropeptide content in DCVs, instead it seems to reduce the clustering of DCVs.

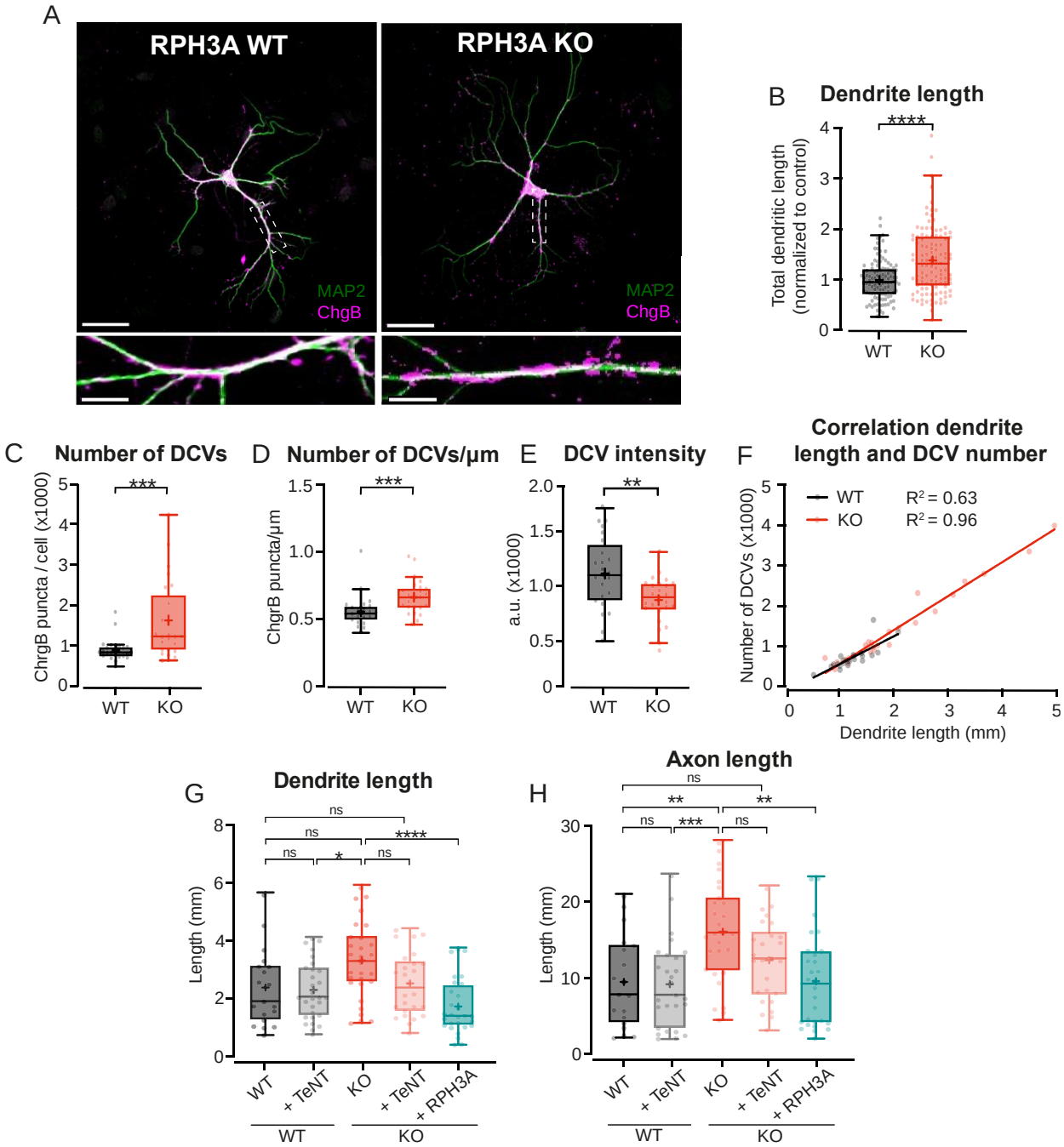

Figure 3. Increased neurite length upon RPH3A deficiency partly depends on regulated secretion. (**A**)Typical example of a single WT and RPH3A KO hippocampal neuron (top) with zooms (bottom) stained for MAP2 (green) and the DCV marker ChgB (magenta). Scale bars, 50 µm (top) and 20 µm (bottom). (**B**) Total dendritic length of single hippocampal RPH3A WT or KO neurons normalized to WT per independent experiment. N numbers per condition: WT: 14(112); KO: 14(113). (**C**) Total number of ChgB labeled DCVs per neuron for each group. N numbers per condition: WT: 3(24); KO: 3(25). (**D**) Total ChgB labeled DCVs per µm for each neuron per group. (**E**) Mean intensity of ChgB labeled DCVs per neuron for each group. (**F**) Correlation between ChgB labeled DCVs and dendritic length (mm). Linear regression goodness of fit (r^2) is given for each group. (**G**) Total dendritic and (**H**) axonal length (mm) of WT and KO neurons - / + TeNT, and KO neurons expressing RPH3A + TeNT. N numbers per condition: WT: 3(19); WT + TeNT: 3(27); KO: 3(28). KO + TeNT: 3(26), KO + RPH3A + TeNT: 3(28). Boxplots represent median (line), mean (+) and Tukey range (whiskers). Each dot represents an individual neuron. Mann-Whitney U or unpaired t test: * $P < 0.05$, ** $P < 0.01$, ***$P < 0.001$, **** $P < 0.0001$. ns = non-significant, $P > 0.05$.

Increased neurite length upon RPH3A deficiency partly depends on regulated secretion

RPH3A deletion resulted in increased DCV exocytosis (Figure 2) and dendrite length (Figure 3B). We reasoned that increased release of neuropeptide- and neurotrophic factors throughout development could contribute to the longer neurites observed. To test this, we inhibited both SV- and DCV fusion by

cleaving VAMP1, VAMP2, and VAMP3 using TeNT (Hoogstraaten et al., 2020; Humeau et al., 2000), followed by immunostainings for MAP2 and Tau to assess dendritic and axonal length, respectively. Neurons infected with TeNT at DIV1 lacked VAMP2 staining at DIV14, confirming successful cleavage (Figure S3A). TeNT expression in WT neurons had no effect on dendritic (Figure 3G) or axonal length (Figure 3H), as shown before (Harms & Craig, 2005). TeNT expression in KO neurons restored neurite length to WT levels. When compared to KO neurons without TeNT, neurite length was not significantly decreased but displayed a trend towards WT levels (Figure 3G, H). Re-expression of RPH3A in KO neurons restored neurite length to WT levels (Figure 3G, H). To identify the downstream pathway, we overexpressed mutant RPH3A constructs, lacking specific interactions (Figure S1A). No differences in dendrite or axon length were observed for any of the mutants compared to WT (Figure S3B, C). These results indicate that the increased neurite length upon RPH3A depletion may depend on regulated secretion.

The SNAP25-, but not RAB3A-interaction domain of RPH3A contributes to limiting DCV exocytosis

To investigate whether the interactions with RAB3A or SNAP25 are relevant to limit DCV exocytosis, we overexpressed FL RPH3A, ΔRAB3A/RAB27A RPH3A (Fukuda et al., 2004), and ΔSNAP25 RPH3A (Ferrer-Orta et al., 2017) in RPH3A KO neurons (Figure 4A). Expression of ΔRAB3A/RAB27A restored DCV fusion and the released fraction of DCVs to WT levels, similar to FL RPH3A (Figure 4B, C). However, expression of ΔSNAP25 did not fully rescue the total number of fusion events or the released fraction of DCVs to WT levels (Figure 4E, F). We did not observe any difference in the number of DCVs upon ΔRAB3A/RAB27A or ΔSNAP25 expression (Figure 4D, G). Taken together, these results suggest that RAB3/27 binding or SNAP25 binding are not essential for the limiting effect of RPH3A on DCV exocytosis, yet the interaction with SNAP25 appears to contribute to this effect.

Discussion

In this study, we addressed the role of RPH3A in DCV exocytosis in hippocampal neurons. RPH3A did not travel with DCVs, instead it predominantly localized at synapses (Figure 1). RPH3A null mutant neurons showed an increase in DCV exocytosis (Figure 2) and had longer neurites that contained more DCVs (Figure 3). The increase in neurite length may partially dependent on regulated secretion, as TeNT expression showed a clear trend towards reduced neurite length to WT levels (Figure 3). Finally, expression of RAB3A/RAB27A-binding deficient, but not a SNAP25-binding deficient RPH3A, in RPH3A KO neurons, restored DCV fusion events to WT levels. (Figure 4). Taken together, we conclude that RPH3A limits DCV exocytosis, partly but not fully through its interaction with SNAP25.

RPH3A does not travel with DCVs in hippocampal neurons

We observed that RPH3A is highly enriched at synapses, as shown before (Li et al., 1994; Mizoguchi et al., 1994; Stanic et al., 2015, 2017). Moreover, RPH3A appeared to be stationary at synapses, as both FL- and truncated RPH3A were highly immobile. In mammalian neurons, the expression levels and localization of RPH3A depend on RAB3 (Schlüter et al., 1999). In line with this, we find that a RPH3A mutant unable to bind RAB3A/RAB27A loses its punctate (synaptic) distribution. This was not the case with a RPH3A mutant unable to bind SNAP25. This confirms that the synaptic enrichment of RPH3A

depends, at least in part, on RAB3A/RAB27A interactions, but not SNAP25. In addition, we observed a faster recovery after photobleaching when RPH3A was unable to bind RAB3A. This indicates that the loss of RAB3A interaction makes RPH3A more mobile. RAB3A was recently identified as a DCV protein that travels with mobile DCVs (Persoon et al., 2019). However, hardly any mobile DCV was found to contain RPH3A. This confirms that RPH3A plays a more significant role within the synapse. In addition,

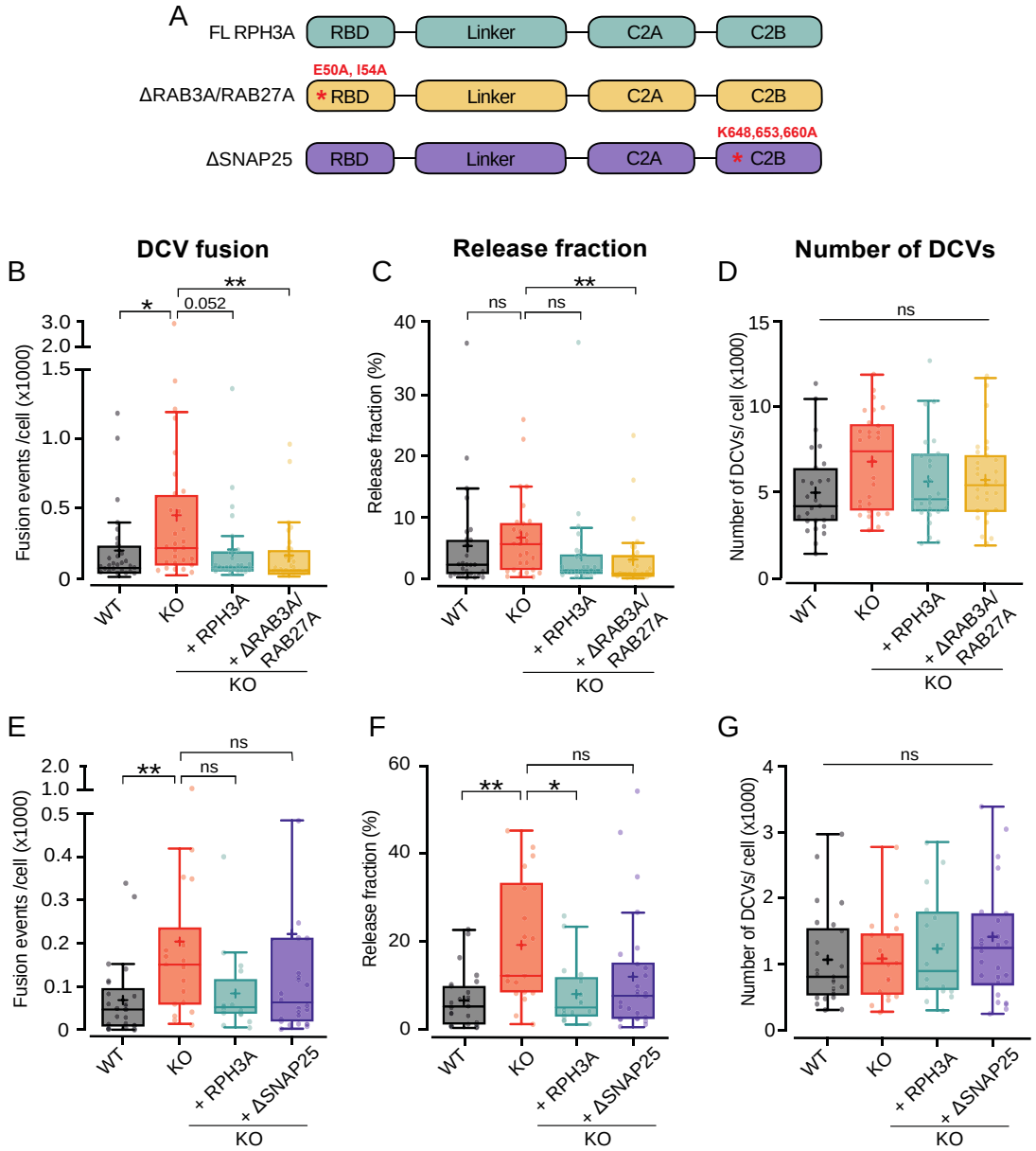

Figure 4. RPH3A interaction with SNAP25, but not RAB3A, partly contributes to limiting DCV exocytosis. (**A**) Domain structure of FL RPH3A (cyan), ΔRAB3A/RAB27A- (yellow) and ΔSNAP25 mutant RPH3A (purple) with the corresponding mutant sites in red. (**B**) Total DCV fusion events in WT (black), KO (red) and KO neurons expressing RPH3A (cyan) or ΔRAB3A/RAB27A RPH3A mutant (yellow). N numbers per condition: WT: 4(27); KO: 4(28); KO + RPH3A: 4(24); KO + ΔRAB3A/RAB27A: 4(28). (**C**) Released fraction of the number of fusion events normalized by the total DCV pool per cell. (**D**) Total NPY-pHluorin labeled DCV pool estimates derived from $NH4^+$ superfusion. (**E**) Total number of DCV fusion events in WT (black), KO (red) and KO neurons expressing RPH3A (cyan) or ΔSNAP25 RPH3A mutant (purple). N number per condition: WT: 4(25); KO: 4(18); KO + RPH3A: 4(16); KO + ΔSNAP25: 4(26). (**F**) Release fraction per cell. (**G**) Total NPY-pHluorin labeled DCV pool per cell. Boxplots show the mean (+), median (line) and Tukey range (whiskers). Each dot represents a single neuron. Kruskal-Wallis H test with Dunn's correction: * $P < 0.05$, ** $P < 0.01$. ns = non-significant, $P > 0.05$.

we showed that RAB3A is necessary for the correct localization of RPH3A, and that the interaction with RAB3A might ensure cluster formation of RPH3A at the synapse. These data do not exclude that RPH3A interacts with immobile DCVs at synapses, potentially in a docked or primed state at the release sites.

This would be in line with our finding that RPH3A serves as a negative regulator of DCV exocytosis. Based on these findings, we propose that RAB3A may recruit RPH3A to DCV release sites, where it may interact with (immobile) DCVs that are primed for release.

RPH3A limits DCV exocytosis in hippocampal neurons

DCV exocytosis was increased by 3-fold upon RPH3A depletion. We were able to rescue this effect by overexpressing FL RPH3A. These results suggest that RPH3A negatively regulates DCV exocytosis. This is in line with *C. elegans* data*,* showing that the lack of the nematode homolog *rbf-1* increased DCV exocytosis, but had no effect on spontaneous release of SVs. This suggests that *rbf-1* limits DCV exocytosis only (Laurent et al., 2018). In addition, expression of FL RPH3A in PC12 cells reduced high KCl-dependent neuropeptide release (Fukuda et al., 2004). In this study, we demonstrated that RPH3A also reduced neuropeptide release in mammalian hippocampal neurons. Our prior estimations in mouse hippocampal neurons indicated that merely 1-6% of the total DCV pool undergo exocytosis upon strong stimulation (Persoon et al., 2018), implying the existence of an inhibitory release mechanism. To our knowledge, RPH3A is the only negative regulator of DCV exocytosis identified so far.

Increased regulated secretion in RPH3A KO neurons might lead to longer neurites

RPH3A KO neurons have longer neurites that correlated with the number of DCVs as shown before (Persoon et al., 2018). In agreement with previous findings (Ahnert-Hilger et al., 1996; Grosse et al., 1999; Osen-Sand et al., 1996), we find that TeNT expression did not affect neurite length of WT neurons, but showed a trend towards shorter neurites in RPH3A KO neurons. This suggests that the increased neurite length in RPH3A KO neurons is, at least partially, driven by TeNT-dependent regulated secretion, in particular VAMP1, 2 or 3 mediated exocytosis. Given that neuropeptides are key modulators of adult neurogenesis (Mu et al., 2010), and that RPH3A depletion leads to increased DCV exocytosis, it is coherent that we observed longer neurites in RPH3A KO neurons.

The partial rescue by TeNT suggests RPH3A-dependent mechanisms that could explain the increase in neuron size besides regulated secretion. RPH3A could control neurite length by regulating the actin cytoskeleton. RPH3A interacts with actin via binding to α-actinin and ß-adducin (Baldini et al., 2005; Coppola et al., 2001; Kato, Sasaki, et al., 1996). *In vitro* experiments showed that RPH3A together with α-actinin can bundle actin (Kato, Sasaki, et al., 1996). Regulation of the actin cytoskeleton has extensively been linked to neurite outgrowth (Meberg & Bamburg, 2000) making it plausable that lack of RPH3A alters actin regulation, resulting in longer neurites.

The limiting effect of RPH3A on DCV exocytosis partially depends on SNAP25 binding

We recently discovered that RAB3 and its effector RIM1 are positive regulators of DCV exocytosis in mammalian hippocampal neurons (Persoon et al., 2019). In contrast, we demonstrated that RPH3A serves as a negative regulator of DCV exocytosis. Given that RPH3A is a downstream effector of RAB3, and that RAB3 is necessary for synaptic RPH3A enrichment, we expected that the interaction with RAB3A plays a role in limiting DCV exocytosis. However, enhanced DCV exocytosis was rescued upon expression of a RPH3A variant that was unable to bind RAB3A/RAB27A, suggesting that the limiting effect of RPH3A on DCV exocytosis is independent on RAB3A interaction. This indicates that even

though RAB3A is important for the localization of RPH3A, RPH3A can still limit exocytosis when its punctate organization is lost, suggesting that the interaction with RAB3A is not rate limiting. One other potential mechanism by which RPH3A could directly limit exocytosis is by limiting SNAP25 availability, as suggested before (Deák et al., 2006). In line with this, we found that expressing mutant RPH3A that lacks SNAP25 binding in KO neurons did not fully restore DCV exocytosis to WT levels, suggesting that RPH3A limits exocytosis by interacting with SNAP25. Based on these findings, we propose that RAB3A plays a critical role in recruiting RPH3A to synaptic exocytosis sites, where RPH3A binds available SNAP25, consequently restricting the assembly of SNARE complexes and thereby inhibiting DCV exocytosis.

Material and methods

Animals

Animals were housed and bred in accordance with Dutch and institutional guidelines. All animal experiments were approved by the animal ethical committee of the VU University/ VU University Medical Centre (license number: FGA 11-03 and AVD112002017824). All animals were kept on a C57Bl/6 background. For RPH3A KO (Schlüter et al., 1999) and WT primary hippocampal neuron cultures, RPH3A heterozygous mice mating was timed and P1 pups were used to dissect hippocampi. Pups were genotyped prior to dissection to select RPH3A KO and WT littermates.

Neuron culture

Primary hippocampal neurons were cultured as described before (De Wit et al., 2009; Farina et al., 2015). In short, dissected hippocampi were digested with 0.25% trypsin (Gibco) in Hanks' balanced salt solution (Sigma) with 10 mM HEPES (Life Technologies) for 20 minutes at 37 °C. Hippocampi were washed, triturated, and counted prior to plating. For single hippocampal neurons, 1000-2000 neurons/ well were plated on pre-grown micro-islands generated by plating 6000 rat glia on 18 mm glass coverslips coated with agarose and stamped with a solution of 0.1 mg/ml poly-D-lysine (Sigma) and 0.7 mg/ml rat tail collagen (BD Biosciences) (Mennerick et al., 1995; Wierda et al., 2007). For continental hippocampal cultures, 20,000 neurons/ well were plated on pre-grown glial plates containing 18 mm glass coverslips. All neurons were kept in neurobasal supplemented with 2% B-27, 18 mM HEPES, 0.25% Glutamax and 0.1% Pen-Strep (all Gibco) at 37 °C and 5% CO_2.

Lentiviral vectors and infections

All constructs were cloned into lentiviral vectors containing a synapsin promoter to restrict expression to neurons. Lentiviral particles were produced as described before (Naldini et al., 1996). NPY-mCherry, NPY-pHluorin and TeNT-IRES-mCherry were described before (Emperador Melero et al., 2017; Nagai et al., 2002). For re-expression of RPH3A in single RPH3A KO neurons, FL RPH3A was cloned into a lentiviral vector containing an IRES-NLS-mCherry to verify infection during live cell experiments. For DCV fusion experiments at DIV14-DIV16, neurons were infected with RPH3A-IRES-NLS-mCherry, RAB3A and RAB27A binding deficient RPH3A with two-point mutations (E50A and I54A) (Fukuda et al., 2004) and SNAP25 binding deficient RPH3A (K648A, K653A and K660A) (Ferrer-Orta et al., 2017) at DIV1-2. The E51A/I54A double mutant of RPH3A was previously validated to lose RAB3A and RAB27A binding

activity (Fukuda et al., 2004), and the K651A/K656A/K663A mutant was shown to not bind rat WT SNAP25 (Ferrer-Orta et al., 2017). We determined the corresponding residues to be mutated in a mouse SNAP25-binding deficient RPH3A construct (K648,653,660A). Neurons were infected with NPY-pHluorin at DIV8-9. For neurite length and co-travel experiments, FL RPH3A, truncated RPH3A (1-375), RAB3/RAB27 binding deficient RPH3A (Fukuda et al., 2004), RPH3A with two point-mutations in the C2B domain (D568N, D574N) and RPH3A phosphorylation deficient (S217A) (Foletti et al., 2001; Fykse et al., 1995) were N-terminally tagged with EGFP or mCherry interspaced by a short glycine linker sequence (Tsuboi & Fukuda, 2005). For neurite length experiments at DIV14, all constructs were infected at DIV1-2. For co-travel experiments at DIV10 constructs were infected at DIV4.

Immunocytochemistry

Cells were fixed with 3.7% paraformaldehyde (PFA, Merck) in phosphate-buffered saline (PBS; 137 mM NaCl, 2.7 mM KCl, 10 mM Na_2HPO_4, 1.8 mM KH_2PO_4, pH 7.4) for 12 minutes at room temperature (RT). Cell were immediately immunostained or kept in PBS at 4 °C. For ChgB immunostainings, cells were permeabilized in 0.5% Triton X-100 (Fisher Chemical) for 10 minutes and blocked with 5% BSA (Acro Organic) in PBS for 30 minutes at RT. For all other immunostainings, cells were permeabilized with 0.5% Triton X-100 for 5 minutes and blocked with 2% normal goat serum (Fisher Emergo) in 0.1% Triton X-100 at RT. Cells were incubated with primary antibodies overnight at 4°C. Alexa fluor conjugated secondary antibodies (1:1000, Invitrogen) were incubated for 1 hour at RT. Coverslips were mounted in Mowiol (Sigma-Aldrich). Primary antibodies used were: polyclonal ChgB (1:500, SySy), monoclonal RPH3A (1:1000, Transduction Labs), polyclonal MAP2 (1:500, Abcam), polyclonal Syn1 (1:1000, #P610), VGLUT1 (1:5000, Millipore), polyclonal Homer 1 (1:300, SySy), polyclonal Tau (1:1000, SySy), monoclonal VAMP2 (1:1000, SySy) and polyclonal mCherry (1:2000, GeneTex).

Imaging

For live cell experiments, neurons were continuously perfused in Tyrode's solution (2 mM CaCl2, 2.5 mM KCl, 119 mM NaCl, 2 mM MgCl2, 30 mM glucose, 25 mM HEPES; pH 7.4) at RT. For DCV fusion experiments, imaging was performed at DIV14-16 with a Zeiss AxioObserver.Z1 equipped with 561 nm and 488 nm lasers, a polychrome V, appropriate filter sets, a 40x oil objective (NA 1.3) and an EMCCD camera (C9100-02; Hamamatsu, pixel size 200 nm). Images were acquired at 2 Hz with AxioVision software (version 4.8, Zeiss). Electrical stimulation was performed with two parallel platinum electrodes placed around the neuron. After 30 seconds of baseline, 2 x 8 (separated by 30 second) or 1 x 16 trains of 50 APs at 50 Hz (interspaced by 0.5 s) were initiated by a Master-8 (AMPI) and a stimulus generator (A-385, World Precision Instruments) delivering 1 ms pulses of 30 mA. NPY-pHluorin was dequenched 50 or 80 seconds after the last stimulation train by superfusing Tyrode's with 50 mM NH4Cl (replacing 50 mM NaCl). For a detailed protocol of DCV fusion analyses see (Moro et al., 2021).

For co-travel experiments, imaging was performed at DIV9-10 on a Nikon Ti-E eclipse microscope with a LU4A laser system, appropriate filter sets, 60x oil objective (NA = 1.4) and EMCCD camera (Andor DU-897). To visualize NPY-pHluorin, neurons were continuously perfused in Tyrode's containing 25 mM NH_4Cl (replacing 25 mM NaCl). Sequential images for both 488 and 561 color channels were acquired for 2 minutes at 2 Hz. After 2 minutes, neurite stretches were photobleached using a galvano laser

scanner to scan a selected area with both lasers at 100% (26.9 μs pixel dwell time). Bleaching was followed by an 8-minute acquisition at 2 Hz in both channels.

For fixed experiments, confocal images were acquired using a Zeiss LSM 510 confocal laser-scanning microscope (40x objective; NA 1.3) and LSM510 software (version 3.2 Zeiss) for co-localisation experiments or a A1R Nikon confocal microscope with LU4A laser unit (40x objective; NA 1.3) and NIS elements software (version 4.60, Nikon) for all other experiments. To determine both dendrite (MAP2) and axon (Tau) length, the whole glial island was visualized by stitching 4 images (604.7 x 604.7 microns).

Analyses

For DCV fusion experiments, 3x3 pixel ROIs were manually placed around each NPY-pHluorin fusion event using ImageJ. An NPY-pHluorin event was considered a DCV fusion event if it suddenly appeared and if the maximal fluorescence was at least twice the SD above noise. Custom written MATLAB (MathWorks, Inc.) scripts were used to calculate the number and timing of fusion events. The total DCV number per neuron was derived from the highest intensity frame during NH_4^+ perfusion of NPY-pHluorin infected neurons. All DCV puncta were selected and counted using SynD (Schmitz et al., 2011; van de Bospoort et al., 2012) software (version 491) running in MATLAB and divided by the mode of the first quartile of puncta intensity values (an estimate for a single DCV) to estimate the total number of DCVs per neuron. For a detailed protocol of DCV fusion analyses see (Moro et al., 2021).

For DCV co-travel experiments, segmented lines were drawn along the neurites and kymographs were created using the KymoResliceWide plugin in ImageJ. Puncta were considered moving if the minimal displacement during the whole 2- or 8-minute acquisition was at least 3/4 microns within a 10 second period. For co-localisation experiments, the Pearson's and Manders' correlation coefficients were determined using the JACoP plugin (Bolte & Cordelières, 2006). The total DCV number per neuron derived from ChgB immunostaining. Neurite lengths were calculated using SynD (Schmitz et al., 2011; van de Bospoort et al., 2012) software.

Statistical analysis

Statistical tests were performed using R or GraphPad Prism. Normal distributions of all data were assessed with Shapiro-Wilk normality tests and Levene's test of homogeneity of variances. Multi-level models were used to account for variance within the animals when variance between animals significantly improved the model (Aarts et al., 2014). To compare two groups, unpaired Student's t-test in the case of normal distributed data or Mann-Whitney U tests for non-parametric data were used. For multiple comparisons the Kruskal-Wallis test was used for non-parametric data followed by Dunn's multiple comparisons test to compare conditions. Data is represented as boxplots (25-75% interquartile range) with the median (line), mean (+) and Tukey whiskers. N numbers represent number of independent experiments, with the number of individual neurons in brackets. Dots in all graphs indicate single neuron observations, unless stated otherwise.

Acknowledgements

This work is supported by an ERC Advanced Grant (322966) of the European Union (to M.V.) We thank Joke Wortel for animal breeding, Robbert Zalm for cloning and producing viral particles, Desiree Schut and Lisa Laan for astrocyte culture and cell culture assistance, Ingrid Saarloos for assistance in protein chemistry.

References

Aarts, E., Verhage, M., Veenvliet, J. V, Dolan, C. V, & Sluis, S. van der. (2014). A solution to dependency: using multilevel analysis to accommodate nested data. *Nature Neuroscience 2014 17:4*, *17*(4), 491–496. https://doi.org/10.1038/nn.3648

Ahnert-Hilger, G., Kutay, U., Chahoud, I., Rapoport, T., & Wiedenmann, B. (1996). Synaptobrevin is essential for secretion but not for the development of synaptic processes. *European Journal of Cell Biology*, *70*(1), 1–11.

Arora, S., Saarloos, I., Kooistra, R., van de Bospoort, R., Verhage, M., & Toonen, R. F. (2017). SNAP-25 gene family members differentially support secretory vesicle fusion. *Journal of Cell Science*, *130*(11), 1877–1889. https://doi.org/10.1242/jcs.201889

Baldini, G., Martelli, A. M., Tabellini, G., Horn, C., Machaca, K., Narducci, P., & Baldini, G. (2005). Rabphilin localizes with the cell actin cytoskeleton and stimulates association of granules with F-actin cross-linked by α-actinin. *Journal of Biological Chemistry*, *280*(41), 34974–34984. https://doi.org/10.1074/jbc.M502695200

Balkowiec, A., & Katz, D. M. (2002). Cellular mechanisms regulating activity-dependent release of native brain-derived neurotrophic factor from hippocampal neurons. *Journal of Neuroscience*, *22*(23), 10399–10407. https://doi.org/10.1523/jneurosci.22-23-10399.2002

Bittins, C. M., Eichler, T. W., Hammer, J. A., & Gerdes, H. H. (2010). Dominant-negative myosin Va impairs retrograde but not anterograde axonal transport of large dense core vesicles. *Cellular and Molecular Neurobiology*, *30*(3), 369–379. https://doi.org/10.1007/s10571-009-9459-2

Bolte, S., & Cordelières, F. P. (2006). A guided tour into subcellular colocalization analysis in light microscopy. In *Journal of Microscopy* (Vol. 224, Issue 3, pp. 213–232). Blackwell Publishing Ltd. https://doi.org/10.1111/j.1365-2818.2006.01706.x

Coppola, T., Hirling, H., Perret-Menoud, V., Gattesco, S., Catsicas, S., Joberty, G., Macara, L. G., & Regazzi, R. (2001). Rabphilin dissociated from Rab3 promotes endocytosis through interaction with Rabaptin-5. *Journal of Cell Science*, *114*(9), 1757–1764.

de Wit, J., Toonen, R. F., Verhaagen, J., & Verhage, M. (2006). Vesicular trafficking of semaphorin 3A is activity-dependent and differs between axons and dendrites. *Traffic*, *7*(8), 1060–1077. https://doi.org/10.1111/j.1600-0854.2006.00442.x

De Wit, J., Toonen, R. F., & Verhage, M. (2009). Matrix-dependent local retention of secretory vesicle cargo in cortical neurons. *Journal of Neuroscience*, *29*(1), 23–37. https://doi.org/10.1523/JNEUROSCI.3931-08.2009

Deák, F., Shin, O.-H., Tang, J., Hanson, P., Ubach, J., Jahn, R., Rizo, J., Kavalali, E. T., & Südhof, T. C. (2006). Rabphilin regulates SNARE-dependent re-priming of synaptic vesicles for fusion. *The EMBO Journal*, *25*(12), 2856–2866. https://doi.org/10.1038/sj.emboj.7601165

Emperador Melero, J., Nadadhur, A. G., Schut, D., Weering, J. V., Heine, V. M., Toonen, R. F., & Verhage, M. (2017). Differential Maturation of the Two Regulated Secretory Pathways in Human iPSC-Derived Neurons. *Stem Cell Reports*, *8*(3), 659–672. https://doi.org/10.1016/j.stemcr.2017.01.019

Farina, M., van de Bospoort, R., He, E., Persoon, C. M., van Weering, J. R. T., Broeke, J. H., Verhage, M., & Toonen, R. F. (2015). CAPS-1 promotes fusion competence of stationary dense-core vesicles in presynaptic terminals of mammalian neurons. *ELife*, *2015*(4). https://doi.org/10.7554/eLife.05438

Ferrer-Orta, C., Pérez-Sánchez, M. D., Coronado-Parra, T., Silva, C., López-Martínez, D., Baltanás-Copado, J. & Verdaguer, N. (2017). Structural characterization of the Rabphilin-3A–SNAP25 interaction. *Proceedings of the National Academy of Sciences*, *114*(27), E5343-E5351.

Foletti, D. L., Blitzer, J. T., & Scheller, R. H. (2001). Physiological modulation of rabphilin phosphorylation. *The Journal of Neuroscience : The Official Journal of the Society for Neuroscience*, *21*(15), 5473–5483. https://doi.org/10.1523/JNEUROSCI.21-15-05473.2001

Fukuda, M., Kanno, E., & Yamamoto, A. (2004). Rabphilin and Noc2 Are Recruited to Dense-core Vesicles through Specific Interaction with Rab27A in PC12 Cells. *Journal of Biological Chemistry*, *279*(13), 13065–13075. https://doi.org/10.1074/jbc.M306812200

Fykse, E., Li, C., & Sudhof, T. (1995). Phosphorylation of rabphilin-3A by Ca2+/calmodulin- and cAMP-dependent protein kinases in vitro. *Journal of Neuroscience*, *15*(3), 2385–2395. https://doi.org/10.1523/JNEUROSCI.15-03-02385.1995

Grosse, G., Grosse, J., Tapp, R., Kuchinke, J., Gorsleben, M., Fetter, I., Höhne-Zell, B., Gratzl, M., & Bergmann, M. (1999). SNAP-25 Requirement for Dendritic Growth of Hippocampal Neurons. *J. Neurosci. Res*, *56*, 539–546. https://doi.org/10.1002/(SICI)1097-4547(19990601)56:5

Guillén, J., Ferrer-Orta, C., Buxaderas, M., Pérez-Sánchez, D., Guerrero-Valero, M., Luengo-Gil, G., Pous, J., Guerra, P., Gómez-Fernández, J. C., Verdaguer, N., & Corbalán-García, S. (2013). Structural insights into the Ca2+ and PI(4,5)P2 binding modes of the C2 domains of rabphilin 3A and synaptotagmin 1. *Proceedings of the National Academy of Sciences of the United States of America*, *110*(51), 20503–20508. https://doi.org/10.1073/pnas.1316179110

Harms, K. J., & Craig, A. M. (2005). Synapse composition and organization following chronic activity blockade in cultured hippocampal neurons. *Journal of Comparative Neurology*, *490*(1), 72–84. https://doi.org/10.1002/CNE.20635

Hartmann, M., Heumann, R., & Lessmann, V. (2001). Synaptic secretion of BDNF after high-frequency stimulation of glutamatergic synapses. *EMBO Journal*, *20*(21), 5887–5897. https://doi.org/10.1093/emboj/20.21.5887

Hoogstraaten, R. I., van Keimpema, L., Toonen, R. F., & Verhage, M. (2020). Tetanus insensitive VAMP2 differentially restores synaptic and dense core vesicle fusion in tetanus neurotoxin treated neurons. *Scientific Reports*, *10*(1), 10913. https://doi.org/10.1038/s41598-020-67988-2

Humeau, Y., Doussau, F., Grant, N. J., & Poulain, B. (2000). How botulinum and tetanus neurotoxins block neurotransmitter release. *Biochimie*, *82*(5), 427–446. https://doi.org/10.1016/S0300-9084(00)00216-9

Kato, M., Sasaki, T., Ohya, T., Nakanishi, H., Nishioka, H., Imamura, M., & Takai, Y. (1996). Physical and Functional Interaction of Rabphilin-3A with α-Actinin *. *Journal of Biological Chemistry*, *271*(50), 31775–31778. https://doi.org/10.1074/JBC.271.50.31775

Kwinter, D. M., Lo, K., Mafi, P., & Silverman, M. A. (2009). Dynactin regulates bidirectional transport of dense-core vesicles in the axon and dendrites of cultured hippocampal neurons. *Neuroscience*, *162*(4), 1001–1010. https://doi.org/10.1016/j.neuroscience.2009.05.038

Laurent, P., Ch'ng, Q. L., Jospin, M., Chen, C., Lorenzo, R., & De Bono, M. (2018). Genetic dissection of neuropeptide cell biology at high and low activity in a defined sensory neuron. *Proceedings of the National Academy of Sciences of the United States of America*, *115*(29), E6890–E6899. https://doi.org/10.1073/pnas.1714610115

Li, C., Takei, K., Geppert, M., Daniell, L., Stenius, K., Chapman, E. R., Jahn, R., De Camilli, P., & Südhof, T. C. (1994). Synaptic targeting of rabphilin-3A, a synaptic vesicle Ca2+/phospholipid-binding protein, depends on rab3A/3C. *Neuron*, *13*(4), 885–898. https://doi.org/10.1016/0896-6273(94)90254-2

Malva, J. O., Xapelli, S., Baptista, S., Valero, J., Agasse, F., Ferreira, R., & Silva, A. P. (2012). Multifaces of neuropeptide Y in the brain - Neuroprotection, neurogenesis and neuroinflammation. In *Neuropeptides* (Vol. 46, Issue 6, pp. 299–308). Churchill Livingstone. https://doi.org/10.1016/j.npep.2012.09.001

Meberg, P. J., & Bamburg, J. R. (2000). Increase in Neurite Outgrowth Mediated by Overexpression of Actin Depolymerizing Factor. *Journal of Neuroscience*, *20*(7), 2459–2469. https://doi.org/10.1523/JNEUROSCI.20-07-02459.2000

Mennerick, S., Que, J., Benz, A., & Zorumski, C. F. (1995). Passive and synaptic properties of hippocampal neurons grown in microcultures and in mass cultures. *Journal of Neurophysiology*, *73*(1), 320–332. https://doi.org/10.1152/jn.1995.73.1.320

Mizoguchi, A., Yano, Y., Hamaguchi, H., Yanagida, H., Ide, C., Zahraoui, A., Shirataki, H., Sasaki, T., & Takai, Y. (1994). Localization of Rabphilin-3A on the Synaptic Vesicle. *Biochemical and Biophysical Research Communications*, *202*(3), 1235–1243. https://doi.org/10.1006/BBRC.1994.2063

Moro, A., Hoogstraaten, R. I., Persoon, C. M., Verhage, M., & Toonen, R. F. (2021). Quantitative analysis of dense-core vesicle fusion in rodent CNS neurons. *STAR Protocols*, *2*(1), 100325. https://doi.org/10.1016/J.XPRO.2021.100325

Mu, Y., Lee, S. W., & Gage, F. H. (2010). Signaling in adult neurogenesis. *Current Opinion in Neurobiology*, *20*(4), 416–423. https://doi.org/10.1016/j.conb.2010.04.010

Nagai, T., Ibata, K., Park, E. S., Kubota, M., Mikoshiba, K., & Miyawaki, A. (2002). A variant of yellow fluorescent protein with fast and efficient maturation for cell-biological applications. *Nature Biotechnology*, *20*(1), 87–90. https://doi.org/10.1038/nbt0102-87

Naldini, L., Blömer, U., Gallay, P., Ory, D., Mulligan, R., Gage, F. H., Verma, I. M., & Trono, D. (1996). In vivo gene delivery and stable transduction of nondividing cells by a lentiviral vector. *Science*, *272*(5259), 263–267. https://doi.org/10.1126/science.272.5259.263

Osen-Sand, A., Staple, J. K., Naldi, E., Schiavo, G., Rossetto, O., Petitpierre, S., Malgaroli, A., Montecucco, C., & Catsicas, S. (1996). Common and distinct fusion proteins in axonal growth and transmitter release. *Journal of Comparative Neurology*, *367*(2), 222–234. https://doi.org/10.1002/(SICI)1096-9861(19960401)367:2<222::AID-CNE5>3.0.CO;2-7

Pang, P. T., Teng, H. K., Zaitsev, E., Woo, N. T., Sakata, K., Zhen, S., Teng, K. K., Yung, W. H., Hempstead, B. L., & Lu, B. (2004). Cleavage of proBDNF by tPA/plasmin is essential for long-term hippocampal plasticity. *Science*, *306*(5695), 487–491. https://doi.org/10.1126/science.1100135

Park, H., & Poo, M. M. (2013). Neurotrophin regulation of neural circuit development and function. In *Nature Reviews Neuroscience* (Vol. 14, Issue 1, pp. 7–23). Nat Rev Neurosci. https://doi.org/10.1038/nrn3379

Persoon, C. M., Hoogstraaten, R. I., Nassal, J. P., van Weering, J. R. T., Kaeser, P. S., Toonen, R. F., & Verhage, M. (2019). The RAB3-RIM Pathway Is Essential for the Release of Neuromodulators. *Neuron*, *104*(6), 1065-1080.e12. https://doi.org/10.1016/j.neuron.2019.09.015

Persoon, C. M., Moro, A., Nassal, J. P., Farina, M., Broeke, J. H., Arora, S., Dominguez, N., Weering, J. R., Toonen, R. F., & Verhage, M. (2018). Pool size estimations for dense-core vesicles in mammalian CNS neurons . *The EMBO Journal*, *37*(20), e99672. https://doi.org/10.15252/embj.201899672

Puntman, D. C., Arora, S., Farina, M., Toonen, R. F., & Verhage, M. (2021). Munc18-1 Is Essential for Neuropeptide Secretion in Neurons. *Journal of Neuroscience*, *41*(28), 5980–5993. https://doi.org/10.1523/JNEUROSCI.3150-20.2021

Schlüter, O. M., Basu, J., Südhof, T. C., & Rosenmund, C. (2006). Rab3 superprimes synaptic vesicles for release: Implications for short-term synaptic plasticity. *Journal of Neuroscience*, *26*(4), 1239–1246. https://doi.org/10.1523/JNEUROSCI.3553-05.2006

Schlüter, O. M., Schmitz, F., Jahn, R., Rosenmund, C., & Südhof, T. C. (2004). A complete genetic analysis of neuronal Rab3 function. *Journal of Neuroscience*, *24*(29), 6629–6637. https://doi.org/10.1523/JNEUROSCI.1610-04.2004

Schlüter, O. M., Schnell, E., Verhage, M., Tzonopoulos, T., Nicoll, R. A., Janz, R., Malenka, R. C., Geppert, M., & Südhof, T. C. (1999). Rabphilin knock-out mice reveal that rabphilin is not required for rab3 function in regulating neurotransmitter release. *The Journal of Neuroscience : The Official Journal of the Society for Neuroscience*, *19*(14), 5834–5846. https://doi.org/10.1523/JNEUROSCI.19-14-05834.1999

Schmitz, S. K., Hjorth, J. J. J., Joemai, R. M. S., Wijntjes, R., Eijgenraam, S., de Bruijn, P., Georgiou, C., de Jong, A. P. H., van Ooyen, A., Verhage, M., Cornelisse, L. N., Toonen, R. F., & Veldkamp, W. (2011). Automated analysis of neuronal morphology, synapse number and synaptic recruitment. *Journal of Neuroscience Methods*, *195*(2), 185–193. https://doi.org/10.1016/j.jneumeth.2010.12.011

Shimojo, M., Courchet, J., Pieraut, S., Torabi-Rander, N., Sando, R., Polleux, F., & Maximov, A. (2015). SNAREs Controlling Vesicular Release of BDNF and Development of Callosal Axons. *Cell Reports*, *11*(7), 1054–1066. https://doi.org/10.1016/j.celrep.2015.04.032

Stanic, J., Carta, M., Eberini, I., Pelucchi, S., Marcello, E., Genazzani, A. A., Racca, C., Mulle, C., Di Luca, M., & Gardoni, F. (2015). Rabphilin 3A retains NMDA receptors at synaptic sites through interaction with GluN2A/PSD-95 complex. *Nature Communications*, *6*(1), 10181. https://doi.org/10.1038/ncomms10181

Stanic, J., Mellone, M., Napolitano, F., Racca, C., Zianni, E., Minocci, D., Ghiglieri, V., Thiolat, M. L., Li, Q., Longhi, A., De Rosa, A., Picconi, B., Bezard, E., Calabresi, P., Di Luca, M., Usiello, A., & Gardoni, F. (2017). Rabphilin 3A: A novel target for the treatment of levodopa-induced dyskinesias. *Neurobiology of Disease*, *108*, 54–64. https://doi.org/10.1016/J.NBD.2017.08.001

Staunton, J., Ganetzky, B., & Nonet, M. L. (2001). Rabphilin potentiates soluble N-ethylmaleimide sensitive factor attachment protein receptor function independently of rab3. *Journal of Neuroscience*, *21*(23), 9255–9264. https://doi.org/10.1523/jneurosci.21-23-09255.2001

Südhof, T. C. (2013). Neurotransmitter release: The last millisecond in the life of a synaptic vesicle. In *Neuron* (Vol. 80, Issue 3, pp. 675–690). Cell Press. https://doi.org/10.1016/j.neuron.2013.10.022

Tsuboi, T., & Fukuda, M. (2005). The C2B Domain of Rabphilin Directly Interacts with SNAP-25 and Regulates the Docking Step of Dense Core Vesicle Exocytosis in PC12 Cells. *Journal of Biological Chemistry*, *280*(47), 39253–39259. https://doi.org/10.1074/jbc.M507173200

van de Bospoort, R., Farina, M., Schmitz, S. K., de Jong, A., de Wit, H., Verhage, M., & Toonen, R. F. (2012). Munc13 controls the location and efficiency of dense-core vesicle release in neurons. *Journal of Cell Biology*, *199*(6), 883–891. https://doi.org/10.1083/jcb.201208024

van den Pol, A. N. (2012). Neuropeptide Transmission in Brain Circuits. In *Neuron* (Vol. 76, Issue 1, pp. 98–115). Neuron. https://doi.org/10.1016/j.neuron.2012.09.014

Wierda, K. D. B., Toonen, R. F. G., de Wit, H., Brussaard, A. B., & Verhage, M. (2007). Interdependence of PKC-Dependent and PKC-Independent Pathways for Presynaptic Plasticity. *Neuron*, *54*(2), 275–290. https://doi.org/10.1016/j.neuron.2007.04.001

Zaben, M. J., & Gray, W. P. (2013). Neuropeptides and hippocampal neurogenesis. In *Neuropeptides* (Vol. 47, Issue 6, pp. 431–438). Neuropeptides. https://doi.org/10.1016/j.npep.2013.10.002

Supplementary figures

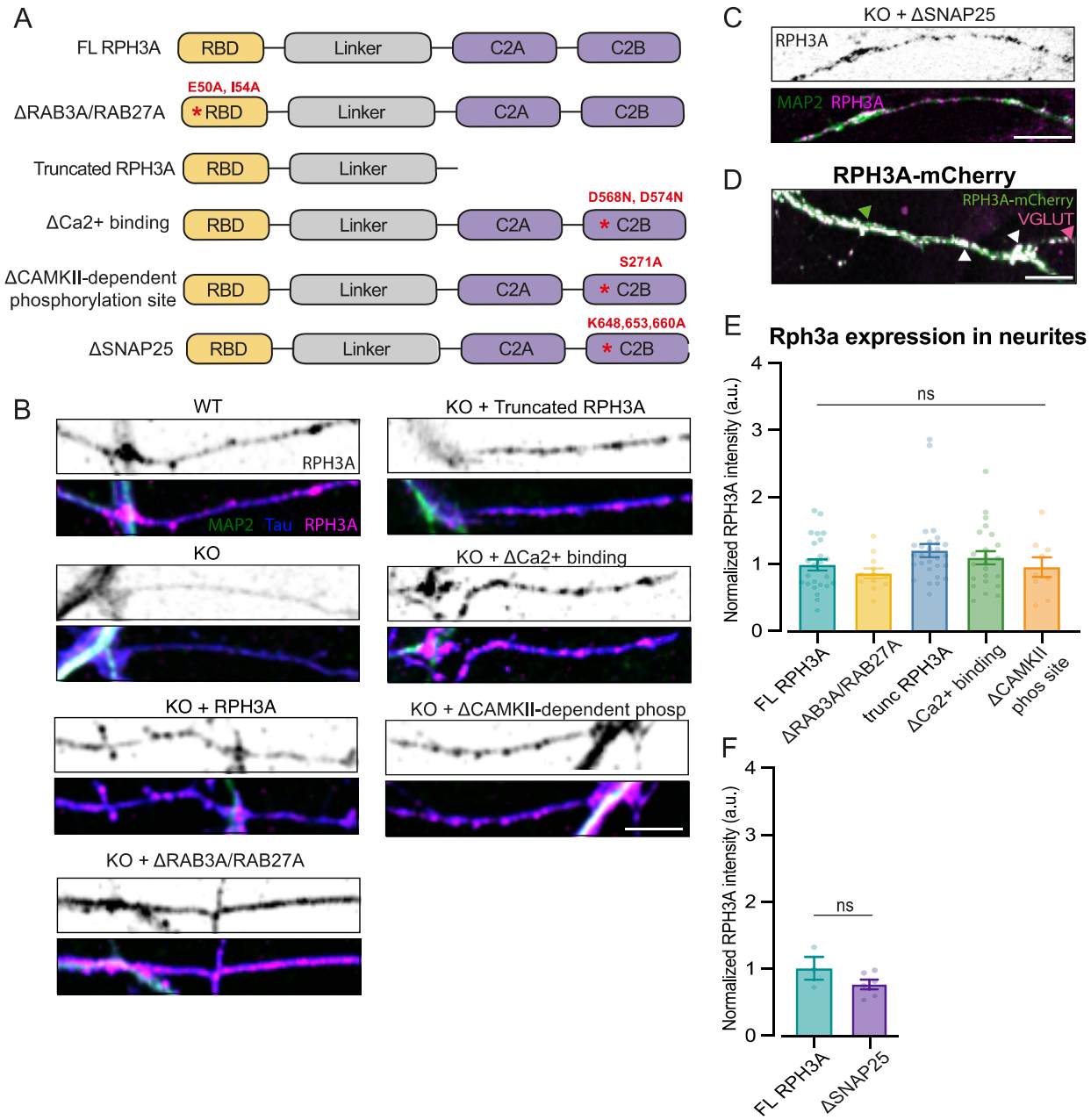

Supplementary figure 1. RPH3A localization depends on RAB3A-binding. (**A**) Domain structures of FL RPH3A and mutant RPH3A constructs lacking specific interactions: ΔRAB3A/RAB27A; truncated RPH3A that lacked its calcium and SNAP25 binding C2A and C2B domain; RPH3A with two C2B domain mutations to reduce calcium binding affinity (ΔCa^{2+} binding); RPH3A that lacked a CaMKII dependent phosphorylation site (ΔCAMKII-dependent phosphorylation site) and ΔSNAP25. The corresponding mutation sites are indicated in red. (**B**) Neurite stretches of WT, KO or KO neurons expressing either FL RPH3A, ΔRAB3A/RAB27A, truncated RPH3A, ΔCa^{2+}-binding and ΔCAMKII-dependent phosphorylation site immunostained for MAP2 (green), Tau (blue) and RPH3A (magenta). Scale bar, 5 µm. (**C**) Neurite stretch of a KO neuron expressing ΔSNAP25 mutant RPH3A immunostained for MAP2 (green) and RPH3A (magenta). Scale bar, 10 µm. (**D**) Neurite stretch of KO neuron expressing RPH3A co-stained for RPH3A (magenta) and VGLUT1 (green). White arrows indicate co-localizing puncta whereas magenta and green arrows indicate single RPH3A or VLGUT1 puncta. Scale bar, 10 µm. (**E**) RPH3A expression in KO neurons expressing FL RPH3A or mutant RPH3A constructs normalized to WT per independent experiment. N numbers per condition: KO + RPH3A: 6(24); KO + ΔRAB3A/RAB27A: 3(12); truncated RPH3A: 6(28); KO + ΔCa2+ binding: 5(23); and KO + ΔCAMKII-dependent phosphorylation: 2(9). (**F**) RPH3A expression in KO neurons expressing FL RPH3A or mutant RPH3A unable to bind SNAP25. N numbers per condition: KO + RPH3A: 1(3); KO + ΔSNAP25: 1(6); Each dot represents a single neuron. Kruskal-Wallis H test with Dunn's correction: ns = non-significant, $P > 0.05$.

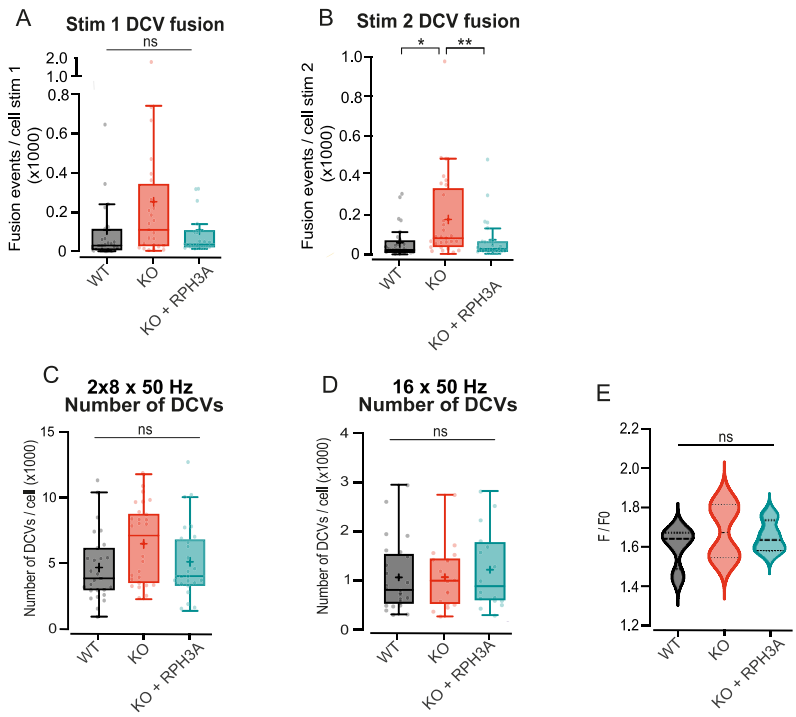

Supplementary figure 2. RPH3A depletion increased DCV exocytosis, but does not affect DCV pool size or content. (**A, B**) DCV fusion events per condition for the first and second 8 x 50 AP bursts at 50 Hz. (**C**) Estimate of the total NPY-pHluorin labeled DCV pool during 2x8 x 50 AP bursts at 50 Hz and (**D**) 16 x 50 AP bursts at 50 Hz. (**E**) Mean peak intensity of NPY-pHluorin during live imaging per independent experiment. The black dashed line represents the median. Boxplots show the mean (+), median (line) and Tukey range (whiskers). Each dot represents a single neuron. Kruskal-Wallis H test with Dunn's correction: * $P < 0.05$, ** $P < 0.01$. ns = non-significant, $P > 0.05$.

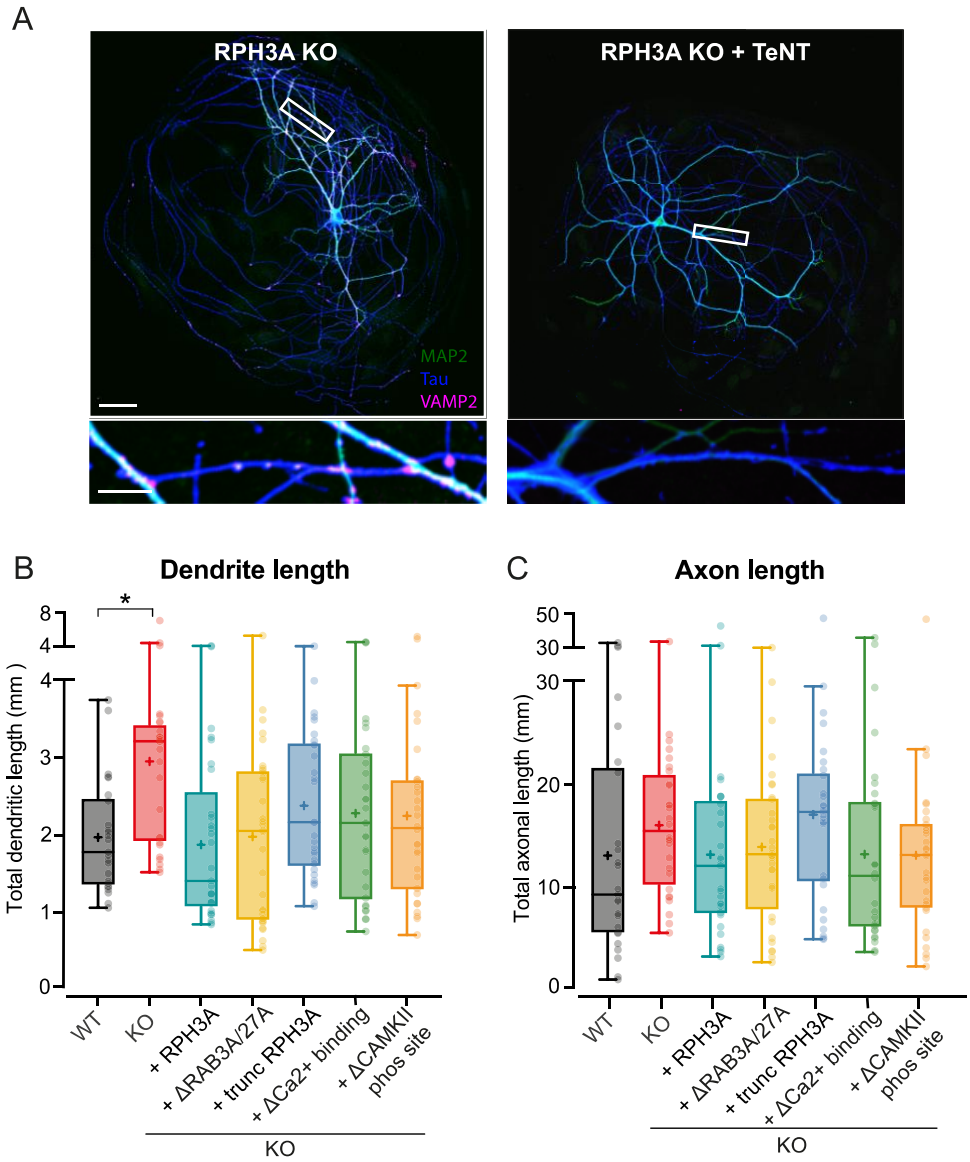

Supplementary figure 3. Increased neurite length upon RPH3A depletion does not depend on RAB3A/RAB27A-binding, calcium binding or phosphorylation of RPH3A. (**A**) Typical example of a single RPH3A WT or KO neuron expressing TeNT with zooms (bottom) stained for MAP2 (green), Tau (blue) and VAMP2 (magenta). Scale bars, 50 µm (top) and 20 µm (bottom). (**B**) Total dendritic and (**C**) axonal length of WT, KO and KO neurons expressing FL or mutant RPH3A (ΔRAB3A/RAB27A, truncated, ΔCa2+ binding or ΔCAMKII-dependent phosphorylation). N numbers per condition: WT 3(25); KO 3(28); KO + RPH3A: 3(29); KO + ΔRAB3A/RAB27A: 3(32); truncated RPH3A: 3(29); KO + ΔCa2+ binding: 3(30); and KO + ΔCAMKII-dependent phosphorylation: 3(30). Each dot represents a single neuron. Kruskal-Wallis H test with Dunn's correction: * $P < 0.05$. ns = non-significant, $P > 0.05$.